Int. J. Electrochem. Sci., 11 **(2016)** 3577 - 3590

International Journal of
ELECTROCHEMICAL
SCIENCE
www.electrochemsci.org

Galvanic Corrosion of Brass /steel 907A Couple in Artificial Seawater

Li Jiang[1,2,*], *Qingsong Yang*[3], *Xiaoqing Du*[1], *Zhen Xu*[1], *Yu Chen*[1], *Zhao Zhang*[1], *Jianqing Zhang*[1],*Chunan Cao*[1]

[1]Department of Chemistry, Zhejiang University, Hangzhou 310027, China;
[2]College of Materials Science and Engineering, China Jiliang University, Hangzhou 310018, China;
[3]Zhanjiang Corrosion and Protection Center, Zhanjiang 524000, China
[*]E-mail: jiangliwhu@126.com

Received: 4 February 2016 / *Accepted:* 3 March 2016 / *Published:* 1 April 2016

Galvanic corrosion of brass /steel 907A couples with various cathode /anode area ratios were examined by electrochemical impedance spectroscopy and electrochemical noise technique. Experimental results show that the galvanic corrosion of couples accelerate within the initial 24h, and then decrease in the later time (from 26h to 720h). The products nucleation, growth, film formation stages are characterized using energy distribution plots (EDP) and two parameters (n_1 and n_2) are adopted to differentiate the nucleation and growth processes. According to the variation tendency of n_1 and n_2, galvanic corrosion process are divided into fluctuating stage and stabilization stage. As the cathode /anode area ratios increase, the corrosion rates of brass /steel 907A couples increase and the period of fluctuating stage lengthens.

Keywords: Galvanic corrosion; Electrochemical noise technique; Brass; Steel 907A

1. INTRODUCTION

Marine metal facility is a system consisting of heterogeneous metals /alloys [1]. Different metals /alloys have different corrosion potentials, if coupled, their potential differences will lead the thermodynamic instability and then accelerate the corrosion rate of more negative side (anode) of the galvanic series. Consequently, offshore facility will has function failure in parts or whole [2]. Steel 907A and brass are two typical materials used in marine metal equipment [3,4], whose corrosion potentials in seawater are -0.66 ~ -0.72 V_{SCE} (hereinafter, V_{SCE} designated the potential referred to the saturated calomel electrode) and -0.243 V_{SCE}, respectively [5]. It suggests that a net potential difference about 0.4 V develops at a junction between steel 907A and brass in the presence of

doi: 10.20964/110437

seawater. In a composite object made of steel 907A and brass parts, steel 907A (more negative side in the galvanic series) becomes the anode and be corroded, while brass becomes the cathode.

So far, the study on galvanic corrosion among dissimilar metals is still a relevant topic [1,3,4]. A number of researches have been conducted to investigate the effects of various operating parameters, such as cathode /anode area ratio [6], temperature [7], dissolved oxygen[8-10], seawater flow rate[11], etc., on the galvanic corrosion. Galvanic corrosion is a dynamic process [12,13], involves several coupled phenomena such as electrochemical reactions, electro-migration, ionic diffusion, oxide layer formation and dissolution [14]. Beyond doubt, during the galvanic corrosion process, an irreversible thermodynamic process accompany with the dissipation of energy will occur meanwhile. Up to now, the energy dissipation regulation in the galvanic corrosion has been researched few [4], moreover, the relationships between crystal energy variation and corrosion process are still unclear [15].

In order to further study the galvanic corrosion mechanism (nucleation /growth of corrosion products, corrosion stages, etc.) and related thermodynamic energy (relative crystal energy and total energy of all the crystals) variation, electrochemical impedance spectroscopy (EIS) and electrochemical noise (EN) technique are adopted. EIS is a global electrochemical method which can provide the vital information (such as corrosion resistance, relative corrosion rate, etc.) of galvanic corrosion process [16]. EN technology is a kind of *in-situ*, non-destructive and local electrochemical technique [15,17]. Using EN technology to study the evolution process of local corrosion in the complex coupling system has the outstanding advantages. In the previous researches of our group [4,16,18-21], local corrosion evolution regulation and corrosion thermodynamic process, as well as its accompanied energy dissipation in other electrochemical system have been clarified thoroughly.

The corrosion potential of metal can demonstrate the reaction tendency and thermodynamic stability in complex corrosion system [22]. According to mixed potential theory [23], brass /steel 907A couples with various cathode /anode area ratios will have different corrosion potential, and hence have different thermodynamic energy. In order to analysis the relationship between crystal thermodynamic energy variation and galvanic corrosion detailed, in this paper, different cathode /anode area ratios were designed.

The present study is aims at investigating the galvanic corrosion between brass and steel 907A with various cathode /anode area ratios by EIS and EN technique. Detailed crystal energy distribution and variation trend affected by cathode /anode area ratios in the galvanic corrosion process were discussed.

2. MATERIALS AND METHODS

2.1 Specimens and solutions

Brass and steel 907A were merchant metals, the chemical composition was displayed in table 1[1,3]. Work-electrodes were fabricated by brass and steel 907A with various cathode /anode area ratios (S_c:S_a) 1:1, 1:3 and 1:9 (see Fig.1). The brass rod of 0.40 cm in diameter was inside, and steel 907A rings intimately contacted with brass outside. The electrode specimens were connected

respectively to a copper wire at one end and sealed using nylon; the other end was exposed as the working surface. Before experiments, the working surface was polished with abrasive papers through 500~1200 grade, washed with distilled water and degreased with acetone.

All tests were carried out in artificial seawater (pH 7.5) at room temperature (25±0.5)°C. The different ions mixed into distilled water and listed in table 2[4].

Table 1. Chemical composition of coupled metals (mass fraction, %; "--"means undetected)

Element / Metal	C	Si	Mn	S	P	Cu	Cr	Ni	Zn	Sn	Pb	Fe
steel 907A	0.12	0.79	1.01	0.007	0.016	0.42	0.64	0.67	--	--	--	--
brass	--	--	--	--	--	61.4	--	--	37.6	0.9	0.007	0.04

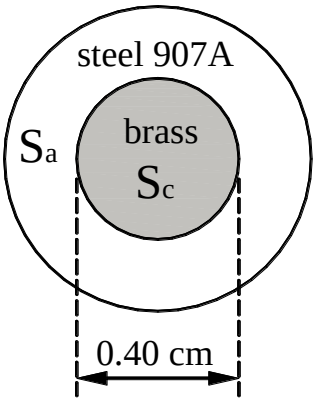

Figure 1. Diagrammatic sketch of electrode sample

Table 2. Chemical composition of artificial seawater

Elements	Cl^-	Br^-	CO_3^{2-}	SO_4^{2-}	Na^+	K^+	Mg^{2+}	Ca^{2+}
Concentration(g/L)	20.237	0.073	1.066	3.237	11.132	0.423	0.137	0.650

2.2. Galvanic corrosion tests and surfaces analysis

Specimens were dipped in still artificial seawater at room temperature for 720 hours. At different test time (such as 10min, 20min, 30min, 4h, 8h, 12h, 24h, etc.), electrochemical impendance spectroscopy (EIS) tests were performed on electrochemical working station (PARSTAT 2273) with applied sinusoidal voltage amplitude 5 mV and sweep frequency from 100 kHz to 0.01Hz. A large platinum foil was used as counter electrode with a saturated calomel electrode (SCE) as reference electrode. Electrochemical noise (EN) was monitored as a function of time between the working electrode and SCE with a Powerlab /4s apparatus (e-DAQ), which was controlled by Chart 4 software using the Windows XP operating system. This equipment allows resolutions of 1 μV for voltage signals and 1 pA for current signals. EN data of 4096 points were collected at 4 point/s each time at

special corrosion process and analyzed with wavelet technique using the orthogonal Daubechies wavelets of the fourth order (db4)[21].

The morphologies of specimens were observed using scanning electron microscope (SEM, JEOL USA JSM-5510LV) with a field emission gun operated at 3.0 kV. The structure and composition were identified by X-ray diffraction (XRD, RIGAKU D /MAX 2550).

3. RESULTS AND DISCUSSION

3.1 EIS analysis

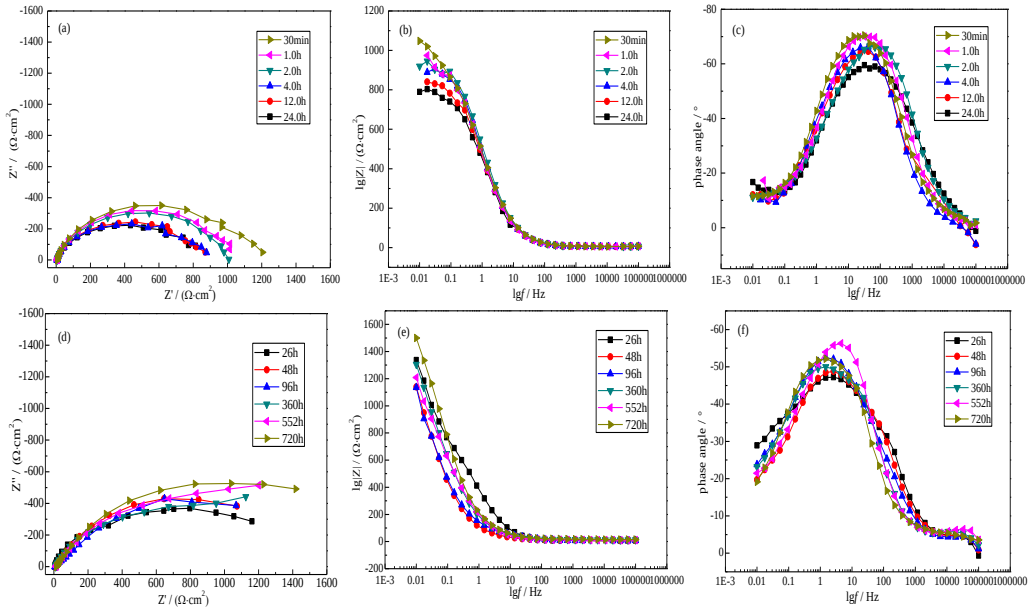

Figure 2. EIS plots of brass /steel 907A couples with cathode /anode area ratio 1:1

Table 3. EIS data for brass /steel 907A couple with cathode/anode area ratio 1:1

Time	R_s/Ω	$CPE_1/\mu F$	n_1	R_{ct}/Ω	$CPE_2/\mu F$	n_2	R_p/Ω
30min	6.626	288.7	0.8602	827.3	--	--	--
1h	6.941	286.4	0.8537	808.5	--	--	--
2h	6.795	280.3	0.8518	798.8	--	--	--
4h	6.839	277.4	0.8342	744.5	--	--	--
12h	6.420	270.8	0.8122	705.5	--	--	--
24h	6.339	274.1	0.8056	678.0	--	--	--
26h	9.009	312.5	0.8044	103.7	54.18	0.8409	711.4
48h	9.405	314.2	0.7484	146.3	56.32	0.8043	729.7
96h	9.953	341.4	0.7609	150.1	71.90	0.8181	753.8
360h	10.990	353.8	0.7557	142.7	78.92	0.8083	771.1
552h	12.322	414.2	0.7484	146.3	76.32	0.8044	729.7
720h	13.845	590.8	0.7851	175.7	85.71	0.8232	884.3

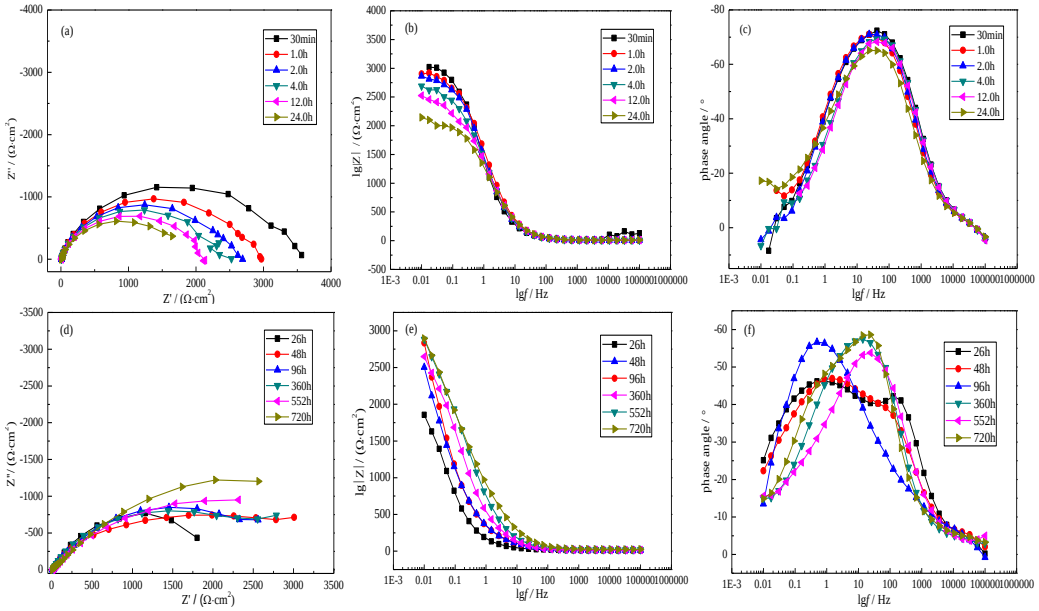

Figure 3. EIS plots of brass /steel 907A couples with cathode /anode area ratio 1:3

Table 4. EIS data for brass /steel 907A couple with cathode /anode area ratio 1:3

Time	R_s/Ω	$CPE_1/\mu F$	n_1	R_{ct}/Ω	$CPE_2/\mu F$	n_2	R_p/Ω
30min	8.23	93.79	0.8544	2544	--	--	--
1h	8.108	90.31	0.8517	2463	--	--	--
2h	8.321	82.22	0.8472	2144	--	--	--
4h	8.028	80.71	0.8504	1967	--	--	--
12h	8.274	79.13	0.8432	1672	--	--	--
24h	8.793	78.94	0.8082	1518	--	--	--
26h	9.919	487.4	0.8038	36.42	101.1	0.7387	2315
48h	9.413	112.4	0.7954	50.35	218.1	0.7920	3342
96h	10.35	120.0	0.8212	43.40	322.5	0.8190	3688
360h	13.65	214.9	0.7781	47.64	349.4	0.8416	3872
552h	13.09	367.9	0.7981	53.91	514.9	0.7906	3978
720h	15.26	438.9	0.8096	51.40	603.8	0.8573	4433

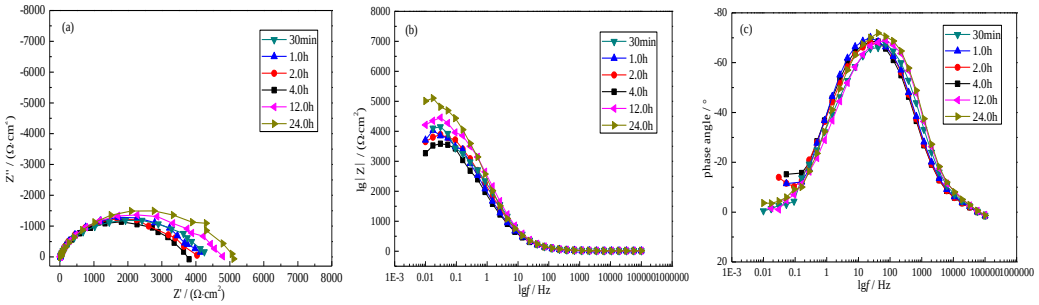

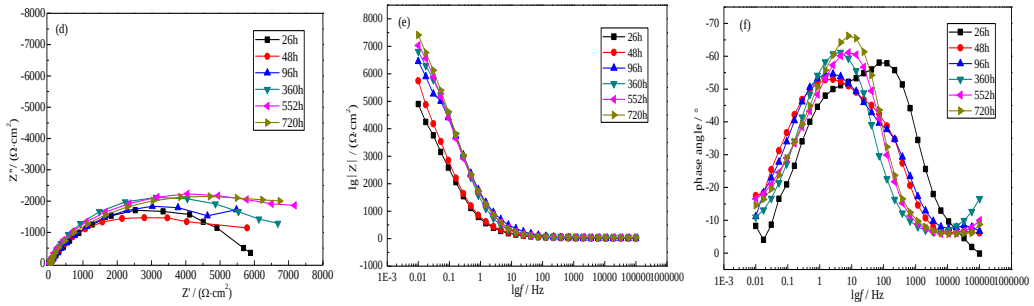

Figure 4. EIS plots of brass /steel 907A couples with cathode/anode area ratio 1:9

Table 5. EIS data for brass /steel 907A couple with cathode /anode area ratio 1:9

Time	R_s/Ω	CPE_1/μF	n_1	R_{ct}/Ω	CPE_2/μF	n_2	R_p/Ω
30min	14.13	73.44	0.8242	3841	--	--	--
1h	13.51	62.39	0.8189	3708	--	--	--
2h	13.49	61.55	0.8154	3413	--	--	--
4h	13.91	63.82	0.8031	3404	--	--	--
12h	13.94	66.07	0.8323	5322	--	--	--
24h	13.51	67.22	0.8556	5884	--	--	--
26h	22.36	112.3	0.8011	45.69	28.47	0.4588	5719
48h	22.19	120.7	0.8083	58.92	35.96	0.4913	6110
96h	21.08	115.6	0.8009	64.20	44.66	0.5170	6670
360h	20.17	123.6	0.8048	78.47	76.47	0.5440	7289
552h	20.46	125.74	0.8292	71.40	96.73	0.6180	7822
720h	19.43	133.18	0.8521	78.92	147.2	0.8060	8028

The galvanic corrosion behaviors of brass /steel 907A couples in artificial seawater have been investigated using EIS technique. The typical EIS evolution features of brass /steel 907A couples with various cathode /anode area ratios are shown in Fig. 3-5. The Nyquist plot is composed of a single capacitance loop and a semicircle, which is attributed mainly to the transient resistance and the double-layer capacitance of the electrode. This also indicates that the charge-transfer process mainly controls the corrosion of galvanic couple [24]. According to the feature of peaks in bode figure and the time constant determine method suggested by Wit [25,26], there is one time constant in the first immersion 24h for brass /steel 907A couple with various cathode /anode area ratios (see figure 2c, 3c and 4c), demonstrating the information of electric double layer capacitance and charge transfer resistance [23]. In this initial stage, corrosion products nucleate and developed gradually. After immersion for 26h, two time constants emerge (see Fig. 2f, 3f and 4f), indicating the characteristics of electric double layer and surface film [4]. The equivalent electrical circuits shown in Fig.5 have been adopted to fit the EIS plots by Z-view software, and the analyzed EIS data were displayed in table 2-4.

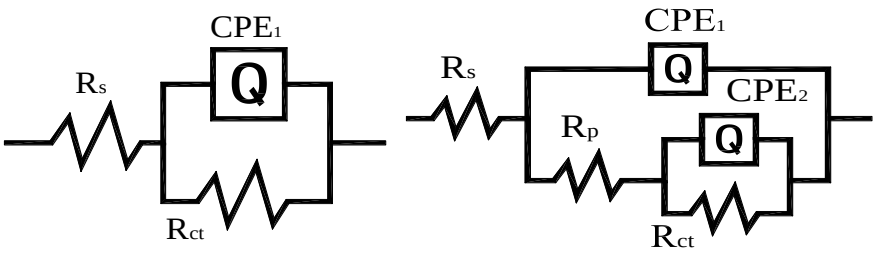

(a) 0-24h (b) 26-720h

Figure 5. Equivalent electrical circuits used for simulating impedance spectra of brass /steel 907A couples with various cathode /anode area ratios immersed in artificial seawater (R_s: solution resistance; CPE_1: the electric double layer capacitance; R_{ct}: charge transfer resistance; CPE_2 and R_p: the capacitance and membrane resistance of outer passivation film and corrosion product layer.)

Within the initial 24h, the capacitance and charge transfer resistance of electric double layer (CPE_1) have the decrease tendency on the surface of galvanic couple with various cathode /anode area ratios. It can be deduced that as the immersion time advance, the original few oxide film on matrix dissolved and corrosion products gradually nucleate/grow to form loose and scattered deposits. From the immersion time 26h to 720h, capacitances of both electric double layer and corrosion product layer increased, which are ascribe to large and thick corrosion products layer covered on matrix surface with time [4].

In order to character the corrosion resistance (R) rationality, the sum of R_{ct} and R_p was adopted [27]. Hence, the corrosion rate was expressed using the reciprocal of this corrosion resistance (R), shown in in Fig.6. As the increase of immersion time, the corrosion rates of galvanic couples with various cathode /anode area ratios increase first (0-24h) and then reduce (26-720h). It can be explained that the former stage is the nucleation /growth process of corrosion products film, with poor protection to matrix; while the later stage is film thickening and stabilization process, penetration of corrosive ions can be hindered to some extent. As the cathode/anode area ratio raise, the corrosion rate of brass /steel 907A couple increase at different immersion time.

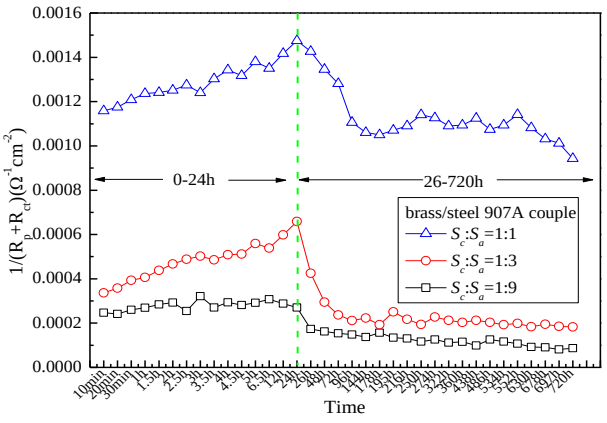

Figure 6. Time dependence of galvanic relative corrosion rates with various cathode /anode area ratios (S_c:S_a)

3.2 EN analysis

Fig.7 shows the potential noise (without elimination of DC drift) of brass /steel 907A couple in artificial seawater for 720h. There is a same variation trend in the brass /steel 907A couples with various cathode /anode area ratios: lower first and then rise slowly. On account of the corrosion products accumulation, dissolution or peeling off from matrix surface, some potential fluctuations appeared. As the cathode /anode area ratio raise, the galvanic potential of couples increased at different immersion time. This same regulation can also be obtained by calculation using mixed potential theory [23].

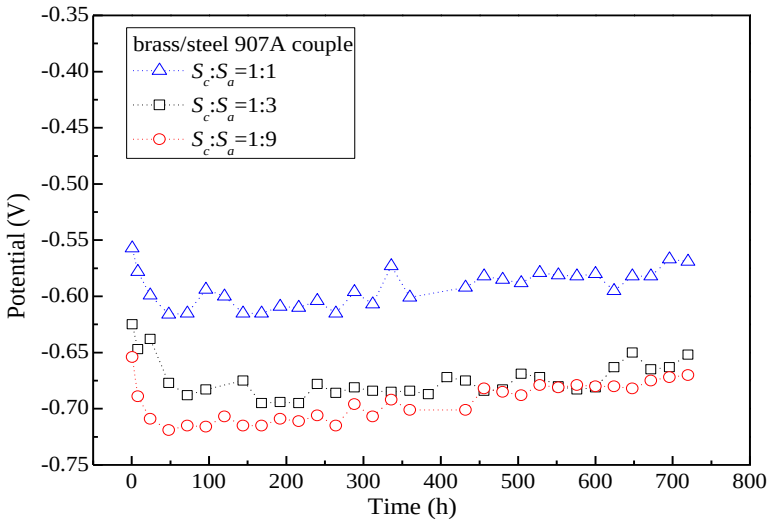

Figure 7. Time dependence of galvanic electrochemical potential noise with various cathode /anode area ratios (S_c:S_a)

The EN data were analyzed with wavelet technique using the orthogonal Daubechies wavelets of the fourth order (db4) [21]. Energy distribution plot (EDP) is used to describe the relationship of the relative energy accumulated by each crystal [23]. In order to eliminate the energy contribution of dc drift from the ensemble energy of the noise, the EDP is re-plotted by discounting the contribution of S_8 crystal from the ensemble signal energy [16,21]. According to the Rp-EDP energy spectra analysis results from the wavelet analysis (Fig.8), the galvanic corrosion process of brass /steel 907A couples immersed in artificial seawaters can be identified into three segments: (1) Nucleation stage. It is a quick reaction. Once the eroded ions diffuse to the matrix surface, pitting corrosion initiates (see Fig. 8a and 8b); (2) Growth stage, including corrosive particle diffusion, autocatalytic corrosion of stable pitting, corrosion products adsorption and precipitation (see Fig. 8c and 8d); (3) Film formation and low diffusion stage. For the autocatalytic corrosion of pitting and enrichment effect of corrosive ions such as Cl^- in the erosion point, more and more corrosion products accumulate on the surface of matrix and form thick product film (see Fig. 8e and 8f).

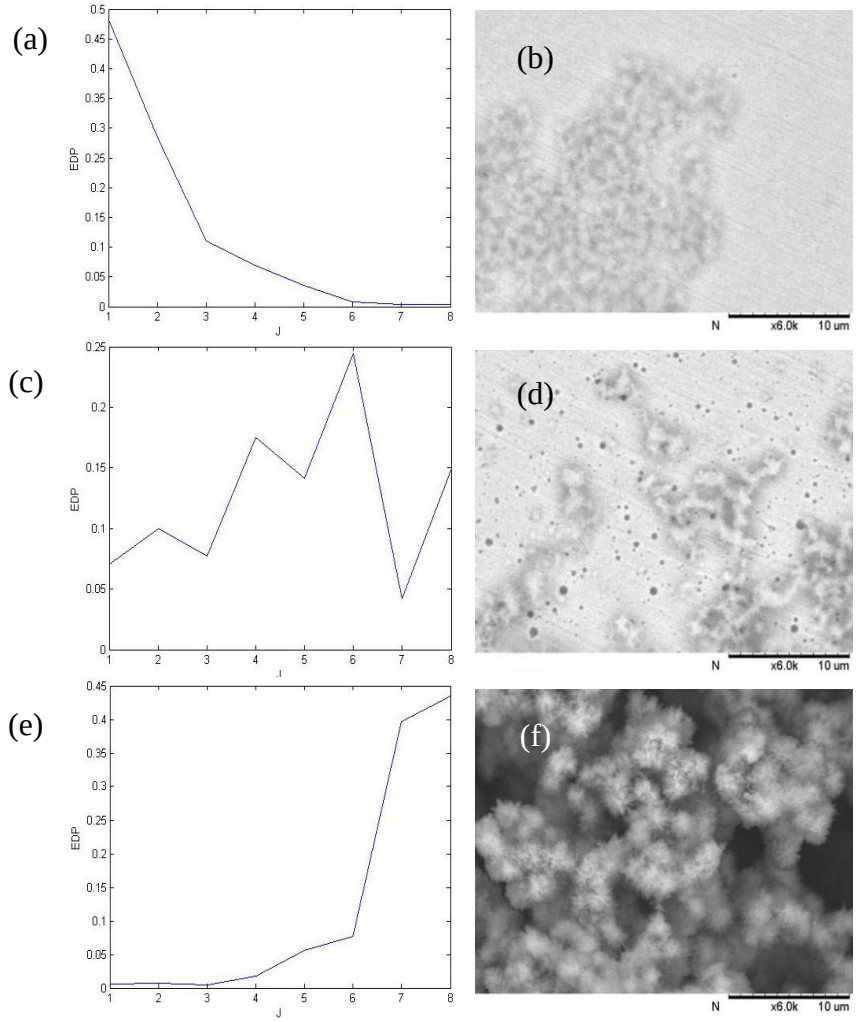

Figure 8. Rp-EDP generated during brass in brass /steel 907A couple corroded in artificial seawater and the corresponding SEM image (e.g. the corrosion process of brass in galvanic couple): (a,b) nucleation; (c,d) growth; (e,f) film formation.

In order to analyze the corrosion evolution features, two new parameters (n_1 and n_2) are defined to differentiate the nucleation and growth processes [21]:

$$n_1 = \frac{Ed1+Ed2+Ed3}{Ed1+Ed2+Ed3+Ed4+Ed5+Ed6} \quad (2)$$

$$n_2 = \frac{Ed4+Ed5+Ed6}{Ed1+Ed2+Ed3+Ed4+Ed5+Ed6} \quad (3)$$

Where (Ed1+Ed2+Ed3) is the nucleation energy, (Ed4+Ed5+Ed6) corresponds to the growth energy. The relationship of the new parameters n_1 and n_2 is plotted in Figure 9. Apparently, the dependences of the two parameters (n_1 and n_2) can be classified into two parts (Fig.9): (a) fluctuating stage (stage I). n_1 and n_2 have some fluctuation and crossing, indicating the nucleation, growing and fall off process of corrosion products; (b) Stabilization stage (stage II). n_1 and n_2 changes slowly with the increase of corrosion time, and the proportion of nucleation energy is higher, indicating the formation of relatively stable films. From the results of Figure 9, it can be seen that as the cathode

/anode area ratios increase (1:9, 1:3 and 1:1), the fluctuating stage (stage I) is longer (160h, 290h and 410h respectively).

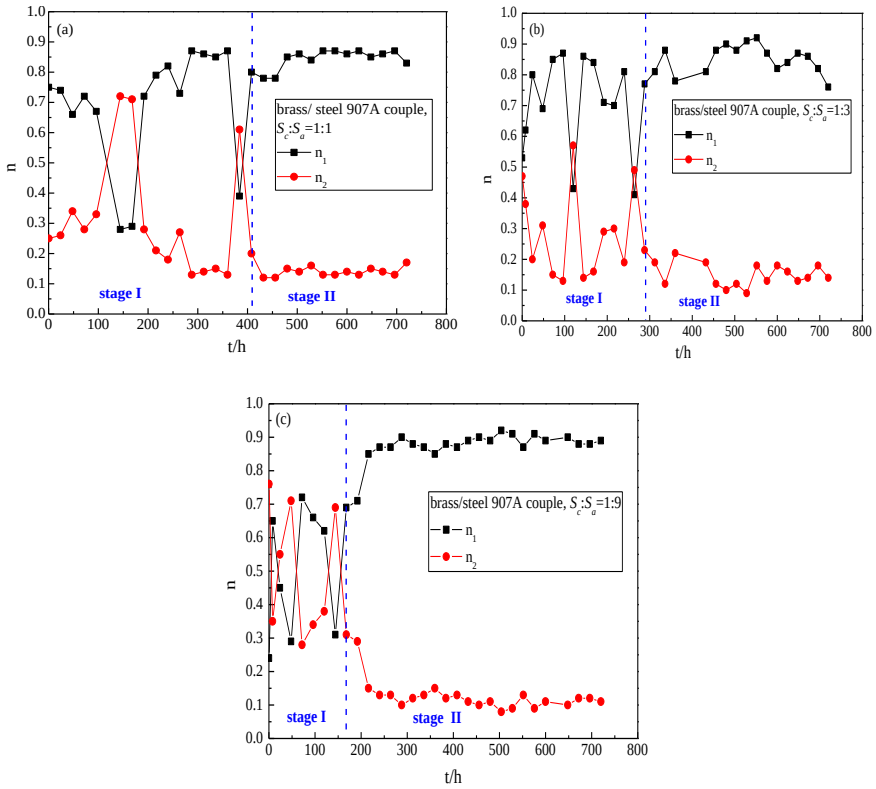

Figure 9. Crystal parameter n_1 and n_2 of brass /steel 907A couples with various cathode /anode area ratios (S_c:S_a) at different immersion time

3.3 Surface and products analysis

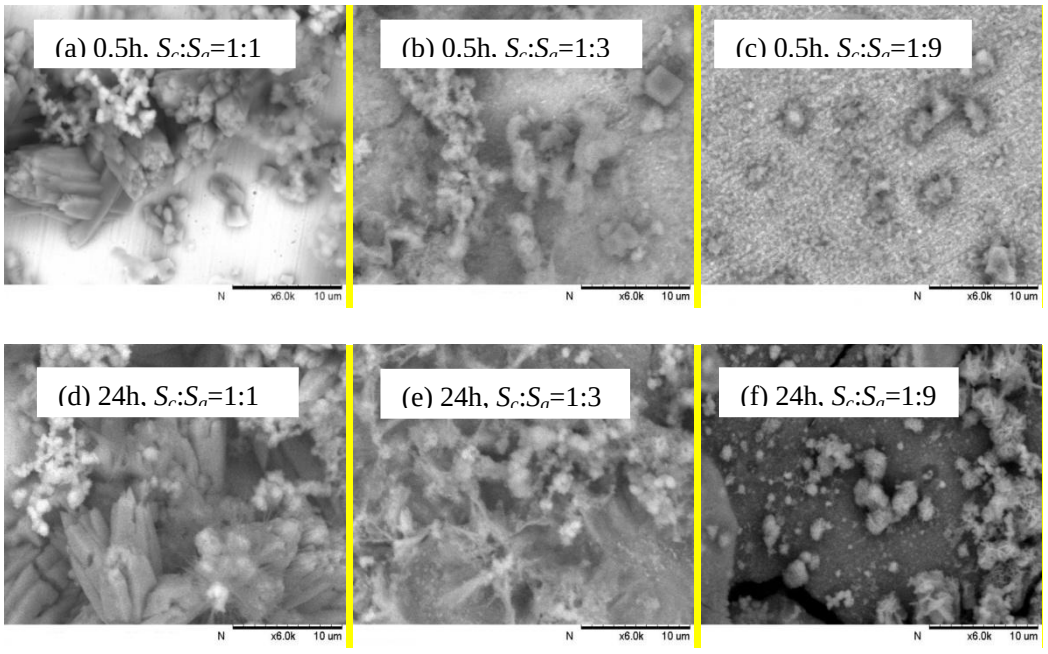

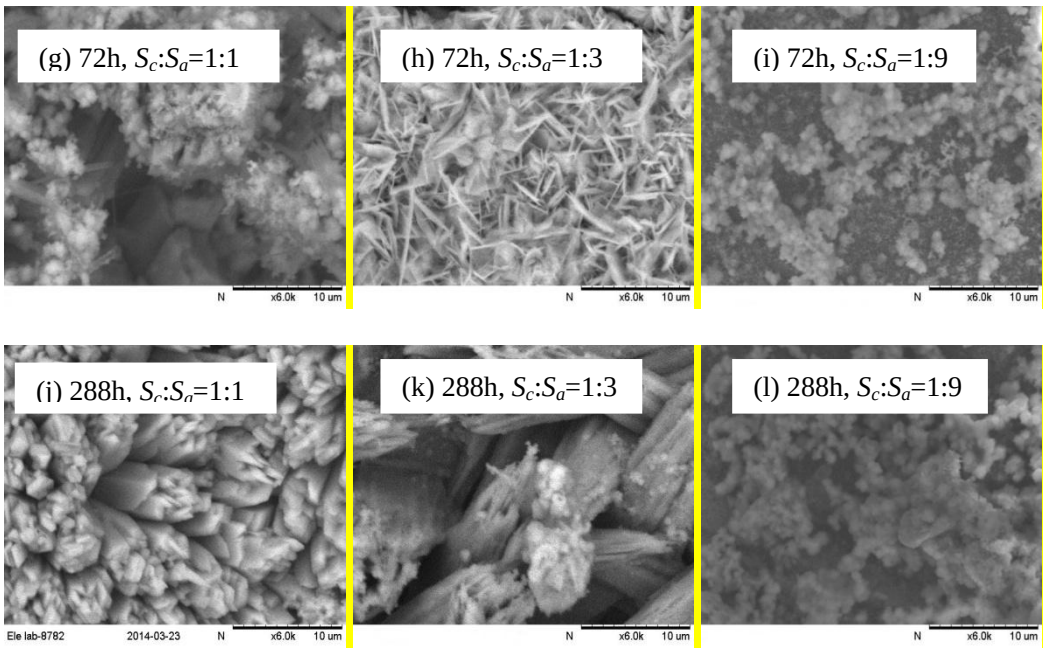

Figure 10. SEM image of steel 907A in brass /steel 907A with various cathode/anode area ratios (S_c:S_a) in artificial seawater

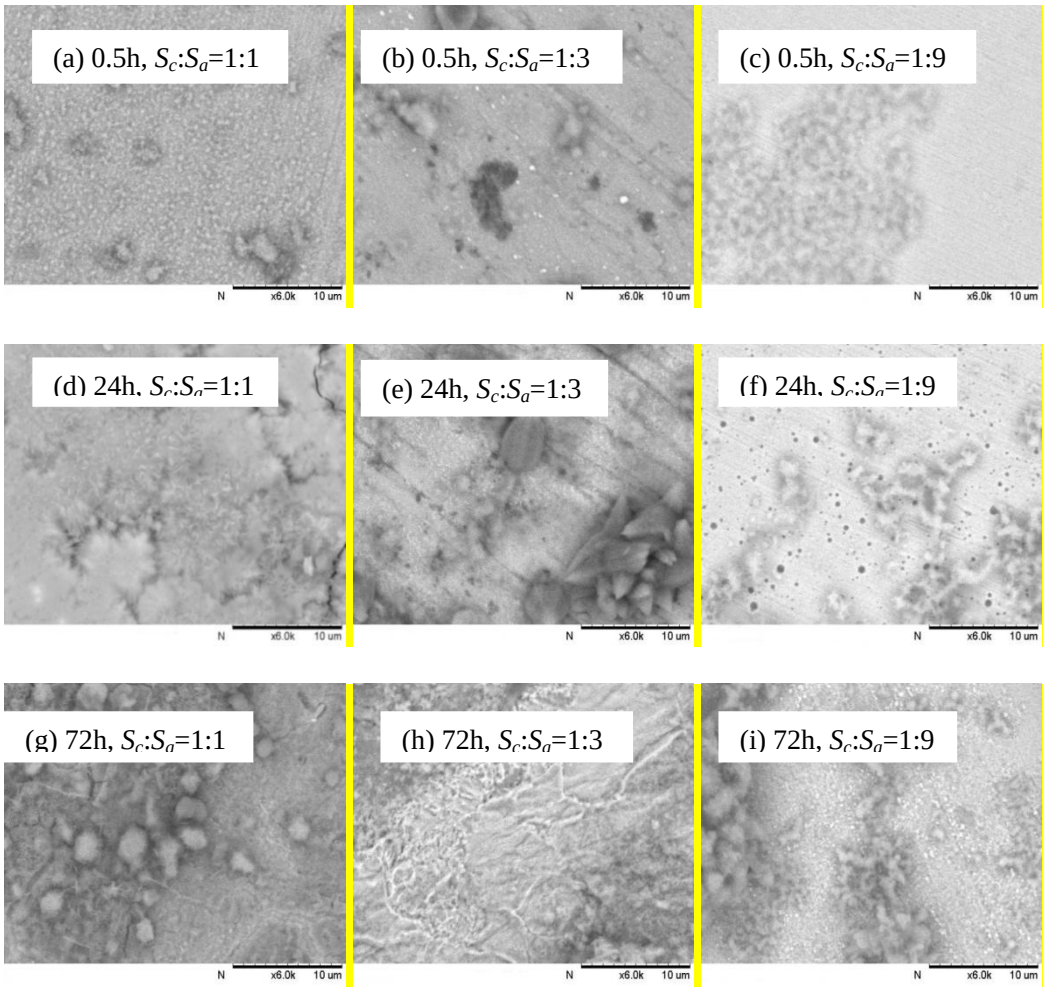

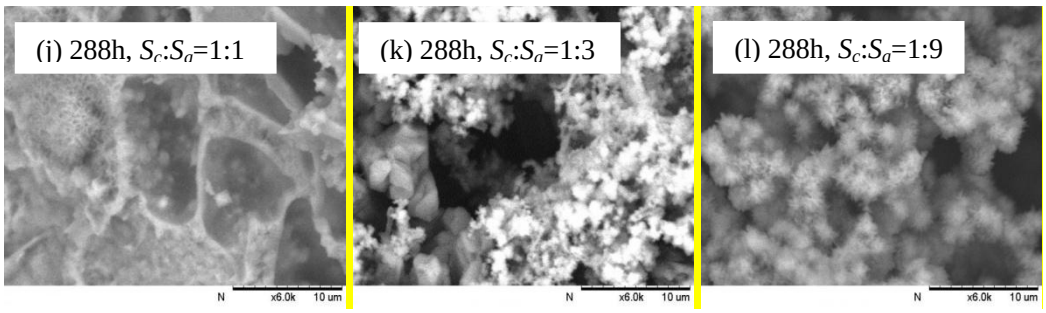

Figure 11. SEM image of brass in brass /steel 907A with various cathode /anode area ratios (S_c:S_a) in artificial seawater

Fig. 10 and 11 show the SEM images of brass and steel 907A in galvanic couple with various cathode /anode area ratios. Once brass /steel 907A couples immersed into the artificial seawaters, the corrosion processes are beginning. For galvanic couple with cathode /anode area ratios, within the first 30min, corrosion pits can be seen on the surfaces of steel 907A (see Fig. 10(a,b,c)), while nearly no color change on brass suface. Under the scanning electron microscope, nucleation/growth of corrosion products can be seen clearly (see Fig.11(a,b,c)). As the immersion time advance, kinds of corrosion products generated. Fig. 12 shows the composition and structure of these corrosion products. There are mainly copper oxide (CuO), iron oxide Hydroxide (FeO(OH)), goethite (FeO(OH)), iron hydroxide ($Fe(OH)_3$) and lepidocrocite (FeO(OH)) on the surface galvanic couples. As the cathode /anode area ratios increase, the corrosion of galvanic surface becomes more and more serious and corrosion products enriched. This change regulation is the same with the research of Dong et al [28].

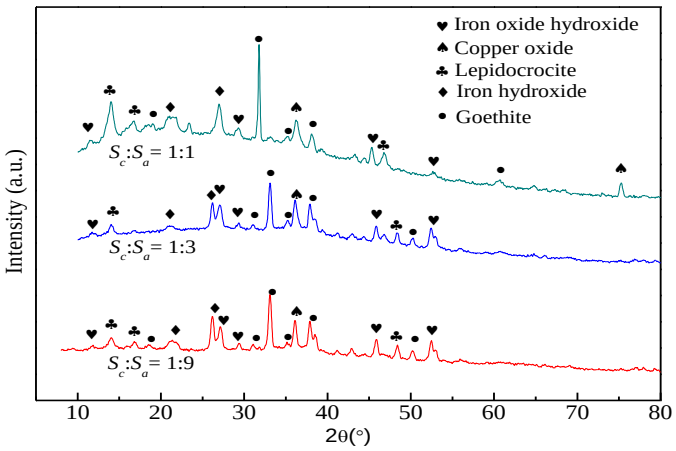

Figure 12. X-ray diffraction patterns of corrosion products on surface of brass /steel 907A couples with various cathode/anode area ratios (S_c:S_a) in artificial seawater

4. CONCLUSIONS

The galvanic corrosion process and mechanism of brass /steel 907A couples with various cathode /anode area ratios in artificial seawater were examined. The results show that within the initial

24h, the corrosion of galvanic couples accelerate; and then decrease in the later time (from 26h to 720h). As the cathode/anode area ratios rise, the corrosion rates increase and more corrosion products (copper oxide, iron oxide Hydroxide, goethite, iron hydroxide and lepidocrocite) generated. The products nucleation, growth, film formation stages can be characterized by energy distribution plot (EDP) from EN analysis. Two parameters (n_1 and n_2) were used to differentiate the nucleation and growth processes and analyze the corrosion evolution features. According to the variation trend of n_1 and n_2, galvanic corrosion process was divided into two stages: fluctuating stage and stabilization stage. As the cathode /anode area ratios increase (1:9, 1:3 and 1:1), the fluctuating stage becomes longer (160h, 290h and 410h respectively).

ACKNOWLEDGEMENTS
This research was supported by the National Natural Science Foundation of China (Grant No. 51401198 and 21403194), China Postdoctoral Science Foundation (Grant No. 2014M560475) and Zhejiang province Postdoctoral Science Foundation (Grant No. BSH1402021).

References

1. M.Du,Q.K. Guo,C.J. Zhou,*J. Chin. Soc. Corros. Prot.*, 26(2006)264.
2. A. A. Khadom, A. F. Hassan, B. M. Abod, *Process Saf. Environ. Prot.*, 98(2015)93.
3. Y.Li, Y.Wang, W.G. Wu, Z.P. Du, Z.B.Li,W. Zhang, *J. Harbin Eng. Univ.*,36(2015)127.
4. X.Q. Du, Q. S. Yang, Y. Chen, Y. Yang, Z. Zhang, *Trans. Nonferrous Met. Soc. China*, 24(2014)570.
5. M.L. Carvalho, J. Doma, M. Sztyler, I. Beech, P. Cristiani, *Bioelectrochem.*, 97(2014)2.
6. Z.S.Tong, W.Zhang, J.Q. Li, J. Gao, J.Q. He, J. Zhou, *J. Univ. Sci. Technol. B.*, 11(2004)127.
7. R. Moshrefi, M. G. Mahjani, A. Ehsani, M. Jafarian, *Anti-corros. Method. M.*, 58(2011)250.
8. F.Bellucci, *Corros.*,47(1991)808.
9. K. A. Lichti, M. Ko, L. Wallis, *Geothermics*, 58(2015)15.
10. M.E. El-Dahshan, A.M.S. El Din, H.H. Haggag, *Desalination*, 142(2002)161.
11. B. O.Hasan, *J. Petrol. Sci.Eng.*, 124(2014)137.
12. A. D. Pergola, F. Lollini, E. Redaelli, L. Bertolini, *Corrosion*, 69(2013)1158.
13. L.L. Machuca, S.I. Bailey, R. Gubner, E.L.J. Watkin, M. P. Ginige, A. H. Kaksonen, K. Heidersbach, *Corros. Sci.*, 67(2013)242.
14. S. K. Thamida, *Comp. Mater. Sci.*, 65(2012)269.
15. M. Sakairia, R. Sasakib, A. Kanekoc, Y. Sekic, D. Nagasawac, *Electrochim. Acta*, 131(2014) 123.
16. X.Q. Huang, Y. Chen, J.Q. Zhou, Z. Zhang, J.Q. Zhang, *J. Electroanal. Chem.*, 709(2013)83.
17. L. Lu, X. G. Li, J. Gao, *Prog. Chem.*, 23(2011)1618.
18. J. M. Li, J. Y. Yin, C. Cai, Z.Zhang, F.H.Cao, J.F.Yang, J.Q.Zhang, *Mater. Corros.*, 63(2012)620.
19. C.Cai, Z. Zhang, Z.L.Wei, J.F. Yang, J.F.Li, *Trans. Nonferrous Met. Soc. China*, 22(2012)970.
20. Y. Y. Shi, Z. Zhang, F. H.Cao, J. Q. Zhang, *Electrochim. Acta*, 53(2008)2688.
21. X. Q. Huang, Y. Chen, T. W. Fu, Z. Zhang, J. Q. Zhang, *J. Electrochem. Soc.*, 160(2013) D530.
22. D.Li, Electrochemical mechanism (third edition), Beijing: Beijing University of Aeronautics and Astronautics Press.2013.
23. J. Q. Zhang, Electrochemical Measurement Technology. Chemical Industry Press, 2010.
24. S. G. Wang, C. B. Shen, K. Long, H. Y. Yang, F. H. Wang, Z. D. Zhang. *J.Phys.Chem.B.*, 109(2005)2499.
25. D. H. van der Weijde, E. P. M. van Westing, J. H. W. de Wit, *Corros. Sci.*, 36(1994)643.

26. P. Campestrini, E. P. M. van Westing, J. H. W. de Wit, *Electrochim. Acta*, 46(2001)2553.
27. H.P.Wang, Y.Chen,J.Zhu,Z.Zhang, J.Q.Zhang, C.N.Cao, the 7th national corrosion congress symposium, 2014,176.
28. C.F.Dong, K.Xiao, X.G.Li, Y.F.Cheng, *Wear*, 270(2010)39-45.

© 2016 The Authors. Published by ESG (www.electrochemsci.org). This article is an open access article distributed under the terms and conditions of the Creative Commons Attribution license (http://creativecommons.org/licenses/by/4.0/).